Deep-Sea Research II 125-126 (2016) 84–95

Contents lists available at ScienceDirect

Deep-Sea Research II

journal homepage: www.elsevier.com/locate/dsr2

Tracing subarctic Pacific water masses with benthic foraminiferal stable isotopes during the LGM and late Pleistocene

Mea S. Cook [a,*], A. Christina Ravelo [b], Alan Mix [c], Ian M. Nesbitt [a,d], Nari V. Miller [a,e]

[a] Geosciences Department, Williams College, 947 Main Street, Williamstown, MA 01267, USA
[b] Ocean Sciences Department, University of California, 1156 High Street, Santa Cruz, CA 95064, USA
[c] College of Earth, Ocean and Atmospheric Sciences, Oregon State University, Corvallis, OR 97331, USA
[d] e4 Sciences, 27 Glen Road, Sandy Hook, CT 06482, USA
[e] School for Earth and Space Exploration, Arizona State University, Tempe, AZ 85287, USA

ARTICLE INFO

Available online 17 February 2016

Keywords:
Paleoclimate
Bering Sea
Oxygen isotope stratigraphy
Pleistocene
Ocean circulation

ABSTRACT

As the largest ocean basin, the Pacific helps to set the global climate state, since its circulation affects mean ocean properties, air–sea partitioning of carbon dioxide, and the distribution of global oceanic poleward heat transport. There is evidence that during the Last Glacial Maximum (LGM) the subarctic Pacific contained a better-ventilated, relatively fresh intermediate water mass above ~2000 m that may have formed locally. The source and spatial extent of this water mass is not known, nor do we know how formation of this water mass varied during Pleistocene glaciations with different orbital and ice sheet boundary conditions. Here we present a 0.5 My multi-species benthic stable isotope record from Site U1345 (1008 m) on the northern Bering slope and a 1.0 My record from U1339 (1868 m) from the Umnak Plateau in the southeastern basin. We find that the relatively well-ventilated low-$\delta^{18}O$ intermediate water reaches 1000 m in the Bering Sea during MIS2, but that the hydrographic divide between this water mass and poorly-ventilated deep water was shallower than 1000 m for earlier glaciations. We also compare Bering Sea piston core and IODP Expedition 323 *Uvigerina* data from the Holocene and LGM with the modern hydrography, and to previously published profiles from the Okhotsk Sea and Emperor Seamounts. We find that the carbon and oxygen stable isotope signatures of well-ventilated water in the Bering and Okhotsk Seas are distinct, suggesting that there may have been intermediate water formation in both basins during the LGM.

1. Introduction

The Pacific contains 50% of the ocean volume (Eakins and Sharman, 2010) and is the largest reservoir of deep water and carbon dioxide in the global ocean. The Pacific circulation state therefore plays a large role in setting the properties of mean ocean water and air–sea partitioning of carbon dioxide. Despite its size, the contribution of the Pacific to the modern global heat transport is relatively small. The heat transport at mid-latitudes associated with North Pacific Intermediate Water (NPIW) ventilation is only 0.1 PW, compared to 0.85 PW associated with the Atlantic Meridional Overturning Circulation (AMOC) (Talley, 2003).

Deep water does not form in the subarctic North Pacific today because of the low salinity of surface water. This low salinity results from limited exchange between the subtropical and subpolar gyres as well as an excess of precipitation over evaporation (Emile-Geay et al., 2003; Warren, 1983), and net freshwater flux from the Atlantic to the Pacific across Central America (Leduc et al., 2007). The deep Pacific is fairly homogeneous deeper than 1000 m, with a maximum in $\Delta^{14}C$ at about 2000 m marking the depth of the oldest Pacific Deep Water (PDW) (Key et al., 2002).

The history of Pacific circulation is poorly understood and consequently, so is its role in glacial–interglacial climate change processes, including sequestration and outgassing of carbon dioxide, heat and freshwater transport, and moisture supply to the atmosphere. In the past, Pacific circulation appears to have been different than today. During the Last Glacial Maximum (LGM), profiles of *Cibicidoides* $\delta^{13}C$ from the western Pacific (Duplessy et al., 1988; Keigwin, 1998; Herguera et al., 1992; Matsumoto et al., 2002) show that there is a hydrographic divide at around 2000 m between an apparently nutrient-depleted well-ventilated water above, and a poorly-ventilated deep water below. The $\delta^{13}C$ and $\delta^{18}O$ data do not constrain the source of this upper water mass, it may have originated locally, it may be Glacial North Atlantic Intermediate Water (GNAIW) transported via the Southern Ocean, or it could be a mixture of water of both Pacific and Atlantic origin

* Corresponding author.
E-mail address: Mea.S.Cook@williams.edu (M.S. Cook).

http://dx.doi.org/10.1016/j.dsr2.2016.02.006
0967-0645/

(Matsumoto et al., 2002). Because of unknown changes in local surface reservoir age in the past, benthic-planktonic radiocarbon measurements from this water mass are ambiguous as to whether it was better ventilated than the modern ocean (Keigwin, 2002).

Today, NPIW ventilates during winter sea-ice formation in the Okhotsk Sea (Shcherbina et al., 2003). The 26.80 σ_θ isopycnal surface at the core of NPIW is very shallow in Gulf of Alaska (MacDonald et al., 2001), suggesting that NPIW may episodically form there as well (Van Scoy et al., 1991). A radiolarian associated with cold, well-ventilated water in the Okhotsk Sea today is most abundant in the Bering Sea during the LGM (Ohkushi et al., 2003; Tanaka and Takahashi, 2005), suggesting that the Bering Sea may have been the source of intermediate water at that time. The εNd measured in bulk-sediment leachates of Fe–Mn oxyhydroxides in the southern Bering Sea is more radiogenic during glaciations, which is also consistent with a North Pacific source of well-ventilated intermediate water (Horikawa et al., 2010). Where does this glacial water mass form? How did it evolve during glacial initiation? How does its volume and mode of formation vary between glacial cycles?

The Integrated Ocean Drilling Program Expedition 323 to the Bering Sea recovered sediment spanning the Pleistocene and Pliocene, allowing systematic investigation of the pattern of glacial–interglacial climate and circulation changes through time as orbital boundary conditions varied. Site U1342 from 819 m from Bowers Ridge in the south-central Bering Sea shows that Pleistocene glaciations are characterized by a relatively high-$\delta^{13}C$, low-$\delta^{18}O$ water mass that may have originated as brine from sea-ice formation in the Bering Sea (Knudson and Ravelo, 2015). In this paper, we present benthic stable isotope stratigraphies from Sites U1345 (1008 m, 60.15°N, 179.50°W) on the northern continental slope and U1339 (1868 m, 54.67°N, 169.98°W) from the southeastern Bering Sea. With these cores, we can trace the depth of the hydrographic divide during glaciations of the late Pleistocene. We also compare a compilation of benthic foraminiferal stable isotope data from the Bering Sea LGM to published data from the Okhotsk Sea.

2. Methods

In U1339 and U1345, we collected two 2-cm half round samples per core section from the primary splice (Takahashi et al., 2011), resulting in a sampling interval of ~75 cm. In U1345, we took additional samples in intervals where lower foraminiferal abundance or preservation resulted in gaps in the stable isotope stratigraphy. We freeze-dried the samples, washed them through a 63 μm sieve with distilled water, then oven-dried them at 50 °C. From the >150 μm size fraction, we picked the benthic foraminiferal species *Uvigerina peregrina*, *U. senticosa* and *Elphidium* cf. *batialis* in U1339, and *U. peregrina, Nonionella labradorica* and *Globobulimina affinis* in U1345.

For each sample, we cleaned 3 tests of each benthic species by sonicating in methanol and deionized water. We measured the U1345 samples and the upper 50 m (CCSF-A) of U1339 at the Oregon State University College of Earth, Oceanic and Atmospheric Sciences Stable Isotope Mass Spectrometer Facility using a Thermo-Finnigan MAT-252 mass spectrometer with a Kiel III carbonate device, using NBS-19 and Wiley (internal calcite lab standard) to correct the data relative to VPDB, with an analytical precision of 0.05‰ for $\delta^{18}O$ and 0.03‰ for $\delta^{13}C$. We measured the remaining U1339 samples at the University of California, Santa Cruz, Stable Isotope Laboratory using a Fisons Prism III mass spectrometer with a common acid bath, and a Thermo-Finnigan MAT-253 mass spectrometer with a Kiel IV carbonate device, using NBS-19 and Carrera Marble (internal calcite lab standard) to correct the data relative to VPDB, with an analytical precision of 0.08‰ for $\delta^{18}O$ and 0.05‰ for $\delta^{13}C$.

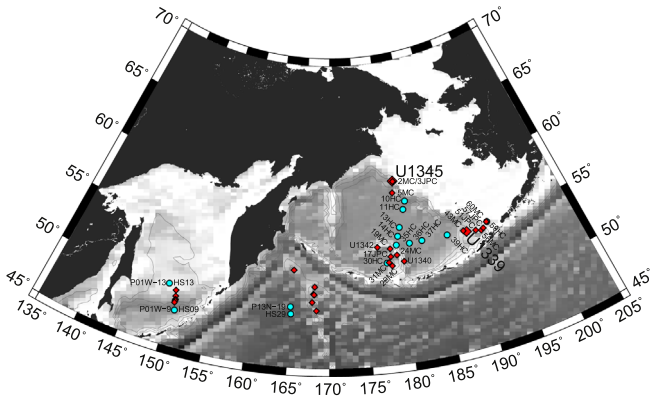

Fig. 1. Map of study area with coring and hydrocast station locations referred to in the text. Large red diamonds show the U1345 and U1339 coring locations, and small diamonds show coring locations for other data from the Bering Sea (see Table 3), and the Okhotsk Sea and Emperor Seamounts (see Keigwin, 1998). The Okhotsk and Emperor hydrostation data are from Keigwin (1998) and WOCE. The bathymetry is from Smith and Sandwell (1997), contour interval is 1000 m. Map made with Generic Mapping Tools (Wessel and Smith, 1998). (For interpretation of the references to color in this figure legend, the reader is referred to the web version of this article.)

In order to compare the sediment data to modern hydrography, we present water column and multicoretop data from samples collected in July, 2002, during HLY02-02 (Fig. 1). See (Lehmann et al., 2005) for hydrostation water collection methods. The $\delta^{13}C$ of dissolved inorganic carbon (DIC) ($\delta^{13}C_{DIC}$) was determined at the National Ocean Science Accelerator Mass Spectrometer (NOSAMS) laboratory at Woods Hole Oceanographic Institution by acidification and automated vacuum extraction of poisoned ~500 mL waters samples, followed by isotope ratio measurements on the NOSAMS VG-PRISM mass spectrometer (McNichol et al., 1994). The standard deviation of replicate extractions and isotopic analyses was 0.04‰ ($n=14$); $\delta^{13}C$ values are reported relative to VPDB. The $\delta^{18}O$ of water ($\delta^{18}O_w$) was determined in the laboratory of D. Schrag (Harvard University) using a VG Optima mass spectrometer with a VG Isoprep 18 automated shaker/equilibrator (Schrag et al., 2002). The standard deviation of replicate $\delta^{18}O$ analyses was 0.02‰ ($n=21$); $\delta^{18}O_w$ values are reported relative to VSMOW.

During HLY02-02, 10-cm-diameter multicorer subcores were sliced at 1 cm intervals, and sediment samples were preserved at sea with a buffered seawater-formalin mixture (Corliss and Emerson, 1990; McCorkle et al., 1997, 1990). In the lab, the 0–1 and 1–2 cm samples were stained with Rose Bengal (1 g/L final concentration) for at least 1 week, and specimens with one or more chambers fully stained a bright pink were picked wet from the >150 mm fraction for isotopic analysis. Between 4 and 6 *Uvigerina,* and 2 to 7 *Cibicidoides* were analyzed on a Finnigan MAT253 mass spectrometer with a Kiel device at the Woods Hole Oceanographic Institution Micropaleontology Stable Isotope Laboratory, using NBS-19 and Carrara Marble (calcite internal lab standard) to correct the data relative to VPDB, with an analytical precision of 0.07‰ for $\delta^{18}O$ and 0.03‰ for $\delta^{13}C$ (Ostermann and Curry, 2000).

We present the $\delta^{18}O_w$ profiles from all Bering Sea hydrocast stations in Fig. 2a, and the CTD T and S in Fig. 2b and c. For comparison, we include the hydrocast data reported in Keigwin (1998) from the Okhotsk Sea and near the Emperor Seamounts (see station locations in Fig. 1). In Fig. 2d, we show the linear least-squares best-fit line between salinity and $\delta^{18}O_w$ for each region. We calculated the equilibrium $\delta^{18}O$ of calcite ($\delta^{18}O_c$) using the CTD T and S of each hydrographic station, applying the regression in

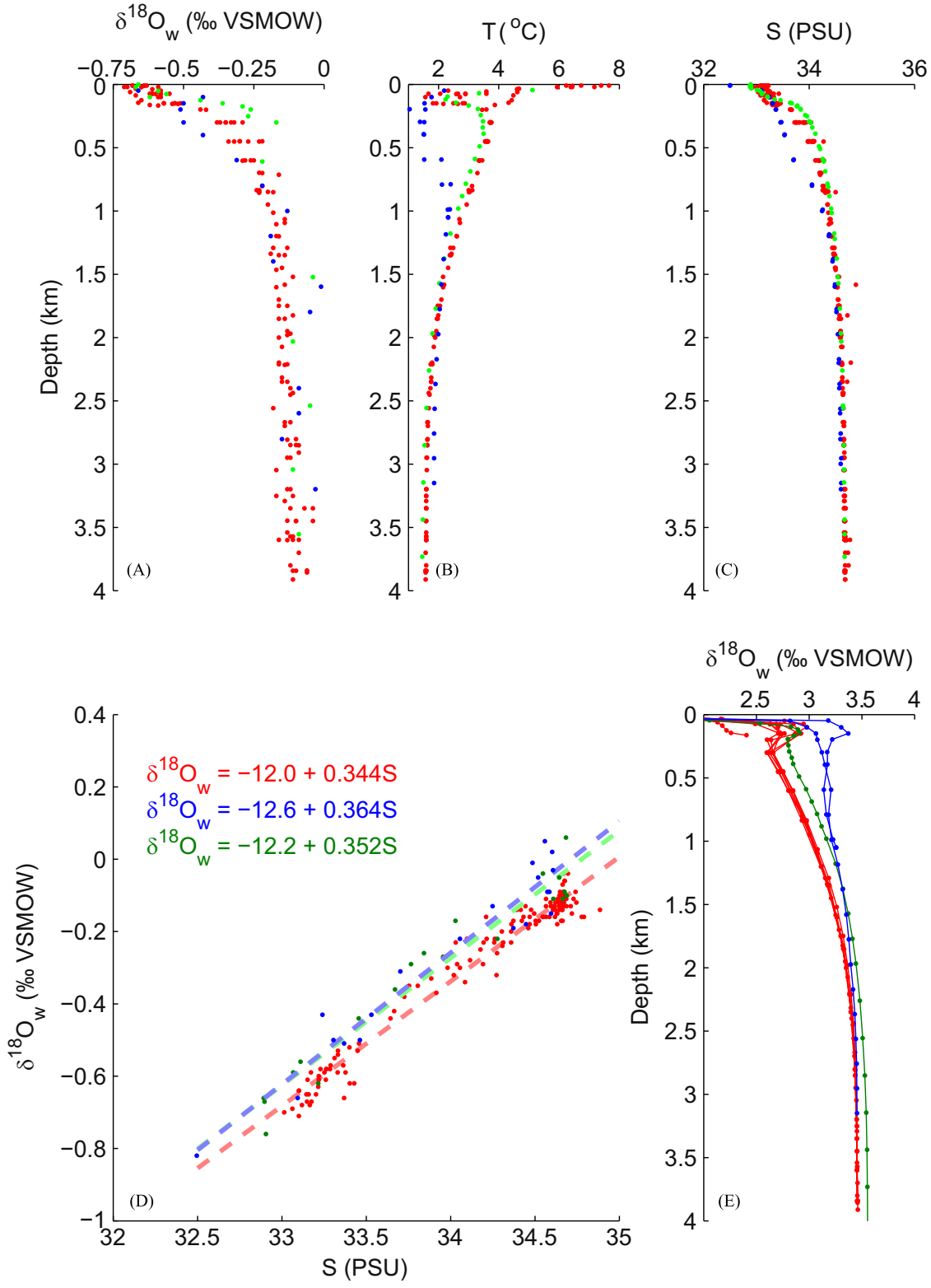

Fig. 2. Hydrocast data from the Bering Sea (red), Okhotsk Sea (blue) and Emperor Seamounts (green). (a, d) The $\delta^{18}O$ of seawater ($\delta^{18}O_w$) and salinity (S) from the hydrocasts from Fig. 1, (b, c) CTD temperature (T) and S. (e) Equilibrium calcite $\delta^{18}O$ ($\delta^{18}O_c$) calculated from the T and S in panels b and c, and the $\delta^{18}O_w$-S relationship in panel d, using Eq. (1) (Shackleton, 1974). (For interpretation of the references to color in this figure legend, the reader is referred to the web version of this article.)

Fig. 2d to get $\delta^{18}O_w$. We used the equation from Shackleton (1974):

$$T = 16.9 - 4.0(\delta^{18}O_C - \delta^{18}O_W), \quad (1)$$

where $\delta^{18}O_W$ and $\delta^{18}O_C$ are relative to VPDB, and T is in Celsius. We converted $\delta^{18}O_W$ from VSMOW to VPDB with $\delta^{18}O_W(\text{VPDB}) = \delta^{18}O_W(\text{VSMOW}) - 0.27$ (Coplen, 1988).

3. Results

3.1. Authigenic carbonates

There are visible authigenic carbonate overgrowths on some samples in U1339, where the foraminiferal tests are yellowish,

which has been observed at many coring sites around the Bering Sea (Cook et al., 2011; Takahashi et al., 2011; Rella et al., 2012; Asahi et al., 2016). These samples have low measured $\delta^{13}C$ (Fig. 3), which is a signature of carbonates associated with anaerobic oxidation of methane (AOM), and is probably not a primary signal recorded from pore water (Herguera et al., 2014). Porewater profiles show that Mg-rich calcite is precipitating in the sulfate–methane transition zone (SMTZ), and that the SMTZ is shallow, at 8–10 mbsf in U1339 and 6–7 mbsf in U1345 (Takahashi et al., 2011; Wehrmann et al., 2011). Though there are several types of authigenic carbonates found in Bering Slope sediments, which form during successive stages of diagenesis, it's likely that the carbonate coatings on foraminifera form during early diagenesis in the SMTZ associated with AOM (Pierre et al., 2016). At sites at the Umnak Plateau, these coatings have been characterized has having very low $\delta^{13}C$ (−22 to −24‰) and high $\delta^{18}O$ (~6.5‰) (Cook et al., 2011).

Since authigenic carbonates are not always visible on samples with anomalous stable isotopes, we flagged samples where the *Uvigerina* and *Nonionella* $\delta^{13}C$ were less than −2.5‰, assuming that such low $\delta^{13}C$ from these shallow infaunal species is an artifact of authigenesis, making both the $\delta^{13}C$ and $\delta^{18}O$ measurements unreliable. The samples that failed this criterion were only in U1339. These points are plotted with open circles in Figs. 3 and 4 and are not shown in Fig. 5. The scatter of flagged samples is consistent with their being a mixture of foraminiferal calcite and authigenic carbonates (Fig. 4a). If we assume the composition of the authigenic carbonates is similar to those observed by Cook et al. (2011), the $\delta^{18}O$ difference between foraminiferal calcite and authigenic carbonates (~3‰) is much smaller than the $\delta^{13}C$ difference (~20‰) (Fig. 4), so even if this filtering by $\delta^{13}C$ does not

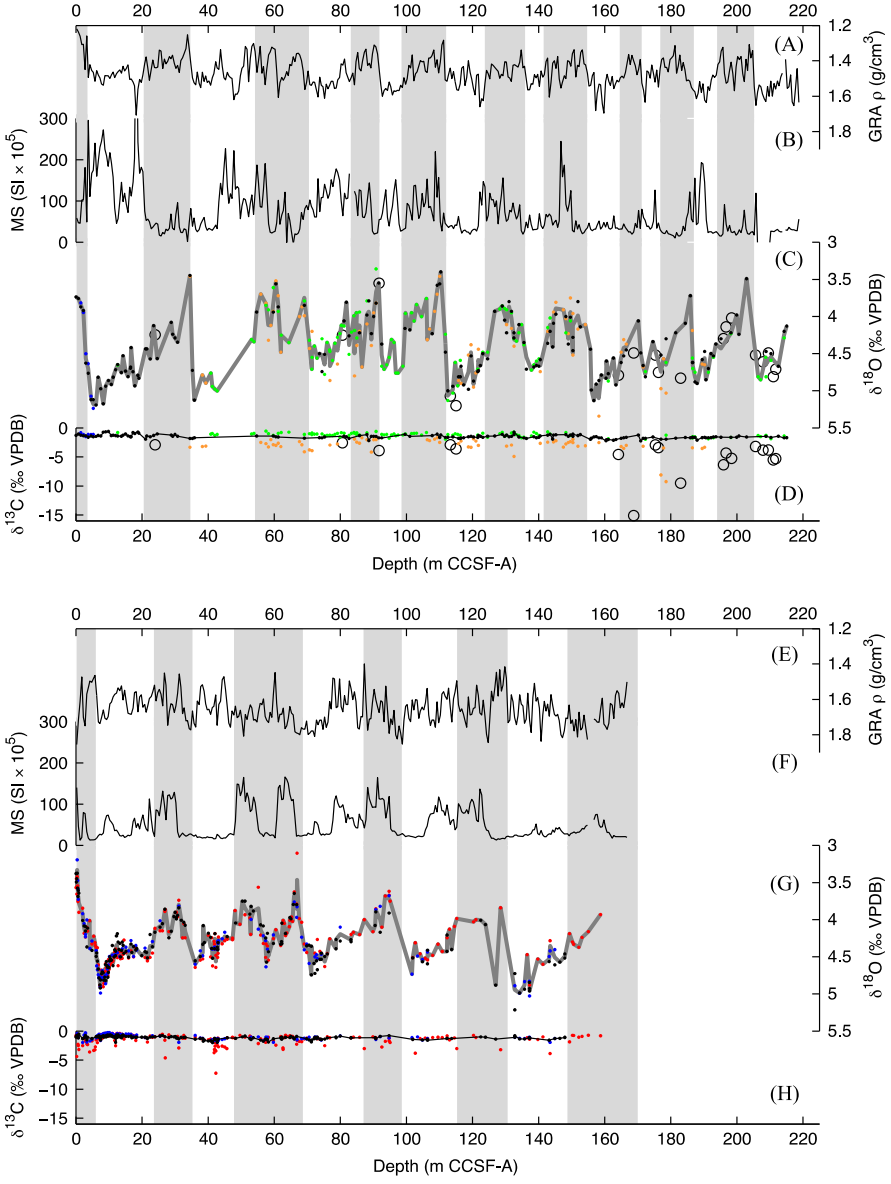

Fig. 3. Benthic stable isotope stratigraphy of U1339 and U1345 based on *U. peregrina* (black), *U. senticosa* (green), *N. labradorica* (blue), *G. affinis* (red) and *E. batialis* (orange). (a, e) Gamma-ray attenuation bulk density, binned at 0.5 m resolution. (b, f) Magnetic susceptibility, binned at 0.5 m resolution. (c, g) Composite $\delta^{18}O$, using the species offset correction from Table 1. The heavy gray line goes through the average value for each sample. (d, h) The benthic $\delta^{13}C$. The thin black line connects the *U. peregrina* data. In panels c, d, g and h, open circles show *Uvigerina* with $\delta^{13}C < -2.5‰$, the isotope data from these samples are not used in calculating species offsets or in the stable isotope stratigraphy. Interglacials according to the age model in Table 2 are shaded in gray. (For interpretation of the references to color in this figure legend, the reader is referred to the web version of this article.)

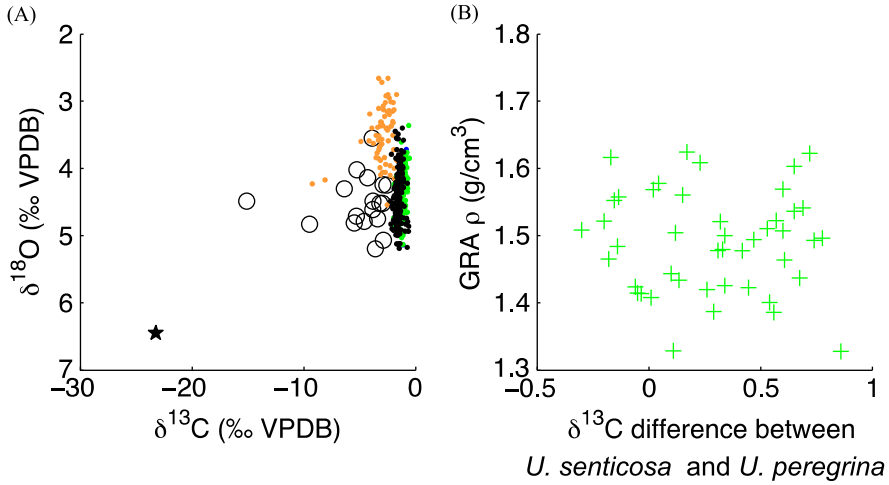

Fig. 4. Assessment of stable isotope data from U1339 (a) Stable isotope measurements. The colors and markers are the same as in Fig. 3, where the *U. peregrina* with $\delta^{13}C < -2.5‰$ are marked with open circles. These filtered data fall roughly in the region of the $\delta^{18}O$–$\delta^{13}C$ plot of mixing between foraminiferal calcite and the composition of authigenic carbonate estimated by Cook et al. (2011) for the Umnak region during MIS3 (star). (b) Comparison of the $\delta^{13}C$ difference between *U. senticosa* and *U. peregrina* and the bulk density, which is a proxy for productivity. There does not appear to be a relationship between productivity and $\delta^{13}C$ difference.

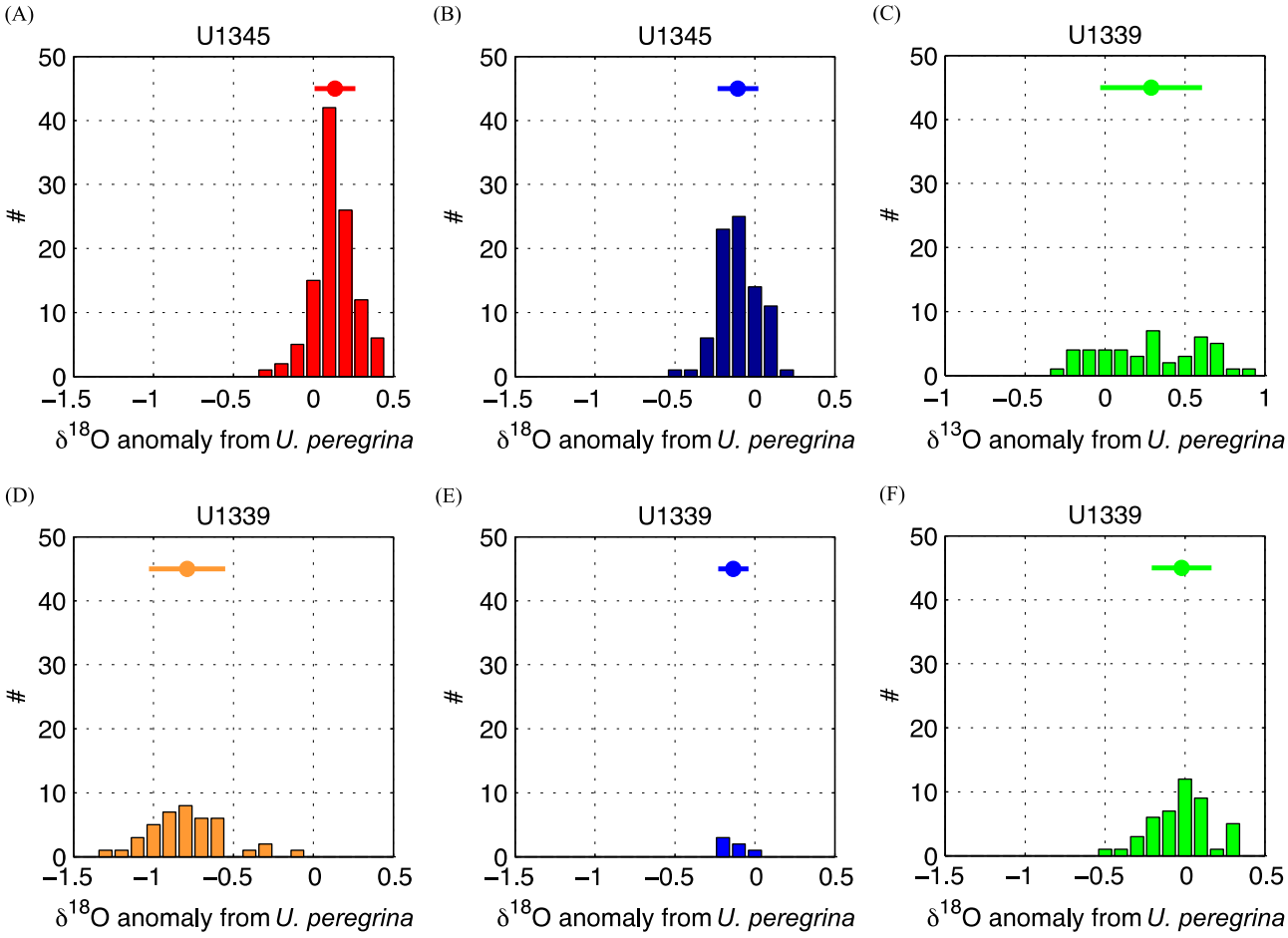

Fig. 5. The offset between *U. peregrina* and other benthic species in samples where multiple species were measured in U1345 and U1339. The mean and standard deviation of the offset for each species (Table 1) are shown in the heavy lines. The colors are the same as in Fig. 3.

capture all samples with authigenic carbonate contamination, the influence on the $\delta^{18}O$ values is probably relatively small. The filtering does, however, clip the $\delta^{13}C$ record, and it's possible that some $\delta^{13}C$ data points that remain are biased by authigenic carbonates.

3.2. Species–species offsets

No one benthic species was present in all samples, so we assembled a multi-species composite $\delta^{18}O$ record. For each sample where we measured multiple species, we plotted the anomaly in

the other species relative to *U. peregrina* (Fig. 5), then calculated the mean and standard deviation of the anomaly (Fig. 5, Table 1) assuming that this vital effect is constant through time. The species–species offsets we observe fall within the 1-sigma uncertainty of the offsets observed by Asahi et al. (2016) for nearby site U1343, and as they note, are consistent with previously published species–species offsets (McCorkle et al., 1997). The stable isotope stratigraphy plotted in Fig. 3a shows the $\delta^{18}O$ measurements corrected for the species–species offsets in Table 1.

The $\delta^{13}C$ of shallow infaunal benthic species are influenced by vital effects as well as differences in depth habitat and the gradient in porewater $\delta^{13}C$ (McCorkle et al., 1990, 1997). We calculated the $\delta^{13}C$ offset only between the related species *U. peregrina* and *U. senticosa* (Fig. 5c) in U1339 (Fig. 5c, Table 1), and applied the correction in Figs. 6–9. To test whether the $\delta^{13}C$ difference between these two species is influenced by changes in productivity affecting porewater $\delta^{13}C$ gradients, we plotted the $\delta^{13}C$ difference with GRA density in U1339 (Fig. 4b) and found there is no relationship. The GRA density in U1339 is driven by opal abundance, a proxy for productivity (Takahashi et al., 2011). In addition, though the productivity increased between the LGM and Holocene in the Okhotsk Sea (Kohfeld and Chase, 2011), the constant $\delta^{13}C$ offset correction between *Cibicioides* and *U. senticosa* (Fig. 8b and d) was sufficient for both time periods, and at a range of depths (1–4 km) where organic matter rain rate presumably also varied. These two lines of evidence suggest that *Uvigerina* $\delta^{13}C$ may be relatively insensitive to variations in productivity.

Table 1
The mean offset of the $\delta^{18}O$ of four benthic species from the $\delta^{18}O$ of *U. peregrina* in samples where both were measured (Fig. 5). This correction is applied to the $\delta^{18}O$ data in Fig. 3.

	U1345 $\delta^{18}O$	U1339 $\delta^{18}O$	U1339 $\delta^{13}C$
U. senticosa		-0.02 ± 0.19 ($n=45$)	0.29 ± 0.32 ($n=45$)
N. labradorica	-0.11 ± 0.13 ($n=82$)	-0.14 ± 0.09 ($n=6$)	
G. affinis	0.13 ± 0.13 ($n=109$)		
E. batialis		$-0.79 \pm .24$ ($n=41$)	

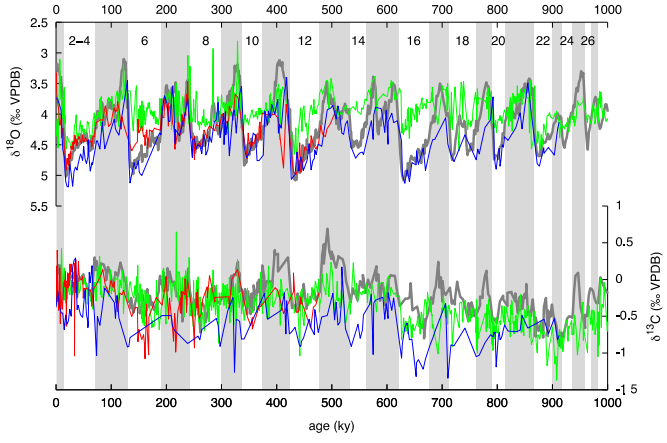

Fig. 6. Stable isotope records from the Bering Sea (U1345, red; U1339, blue; U1342, green) compared to the global benthic $\delta^{18}O$ stack (Lisiecki and Raymo, 2005) in gray in the top panel and a *Cibicidoides* stable isotope record from the eastern equatorial Pacific (Mix et al., 1995) in gray in the lower panel. The interglacials (Lisieicki and Raymo, 2005) are shaded in gray. The U1342 data are from Knudson and Ravelo (2015). We correct the *Uvigerina* $\delta^{13}C$ data by +0.9‰ (Mix, 1995). (For interpretation of the references to color in this figure legend, the reader is referred to the web version of this article.)

3.3. Age model

We identified the Marine Isotope Stages in the stable isotope records by selecting depths at the mid-point of transitions between glacials and interglacials in comparison to the global stack (Lisiecki and Raymo, 2005) (Table 2). In U1339, we also used the GRA density as a guide to selecting the depths of glacial terminations (Fig. 3a), since they are usually associated with an abrupt decrease in density (Takahashi et al., 2011). In U1345, the age model shows that the relationship between magnetic susceptibility (MS) and glacial cycles is complex, but that glaciations are generally associated with lows in MS, and interglacials with highs in MS (Fig. 3f). The U1339 sediment record extends ~1.0 My to MIS23 and U1345 extends ~0.5 My to MIS13.

Microfossil preservation was generally poorer in U1345 than the other sites and the lower abundance of foraminifera in U1345 during deglaciations and peak interglacials mean that the timing of the deglaciation is not well constrained for terminations 2, 4 and 5. For the same reason, we do not capture the minimum $\delta^{18}O$ from peak interglacial MIS 5 or the maximum $\delta^{18}O$ from MIS 6, and may not capture the minima in MIS 9 and 11. The estimated uncertainty in the identification of stage boundaries in Table 2 varies depending on sample spacing during the transitions. Because of unknown phase relationships between the global benthic $\delta^{18}O$ stack, local $\delta^{18}O$, and in U1339 the presumably productivity-driven density changes, the uncertainty in the age of stage boundaries is probably several thousand years.

3.4. Downcore comparisons

We compare the U1345 (1008 m) and U1339 (1868 m) composite $\delta^{18}O$ records with the *U. peregrina* $\delta^{18}O$ record from U1342 (Fig. 6) from 819 m on Bowers Ridge (Knudson and Ravelo, 2015) and the global benthic $\delta^{18}O$ stack (Lisiecki and Raymo, 2005). With the exception of MIS22, the $\delta^{18}O$ difference between the shallowest (U1342) and deepest (U1339) sites during glaciations is larger than 0.3‰ (the modern $\delta^{18}O_c$ difference between these depths), with the difference ranging from 0.4‰ to 0.8‰ (Fig. 7 and Table 4). For the length of the record, U1345 (1008 m) $\delta^{18}O$ falls between the two other sites, but is indistinguishable from U1339 for MIS 8, 10 and 12. During MIS 2, U1345 $\delta^{18}O$ is 0.4‰ lower than U1339. The glacial maximum $\delta^{18}O$ for MIS 6 is not captured because of low sample resolution during the glacial so is not included in Fig. 7 or Table 4.

We plot the *U. peregrina* $\delta^{13}C$ records from U1339, U1345 and U1342 with the *Cibicidoides* $\delta^{13}C$ record from ODP849 in the east equatorial Pacific (Mix et al., 1995), after applying a +0.9‰ correction to the *Uvigerina* data (Mix et al., 1995) (Fig. 6). The minimum $\delta^{13}C$ values in U1339 may be clipped because of the filtering we did to eliminate samples affected by low-$\delta^{13}C$ authigenic carbonates. For this reason, and also since *U. peregrina* does not appear in each sample, careful comparison of the downcore $\delta^{13}C$ records between Bering Sea sites is not possible. However, there does not appear to be a systematic offset between Bering Sea sites during glacials or interglacials.

3.5. Modern and Holocene depth profiles

The modern water column profiles of $\delta^{18}O_C$ and $\delta^{13}C_{DIC}$ at Bering Sea and Emperor Seamounts are similar in shape and amplitude at depths greater than 500 m (Fig. 8). There is increasing $\delta^{18}O_C$ with depth below 500 m due to a combination of increasing $\delta^{18}O_W$ and decreasing T, with most of the change above 2000 m. The Bering Sea $\delta^{13}C_{DIC}$ and $\delta^{18}O_C$ are slightly lower than the values at Emperor Seamounts, consistent with the higher regenerated nutrient and lower oxygen concentrations, as well as

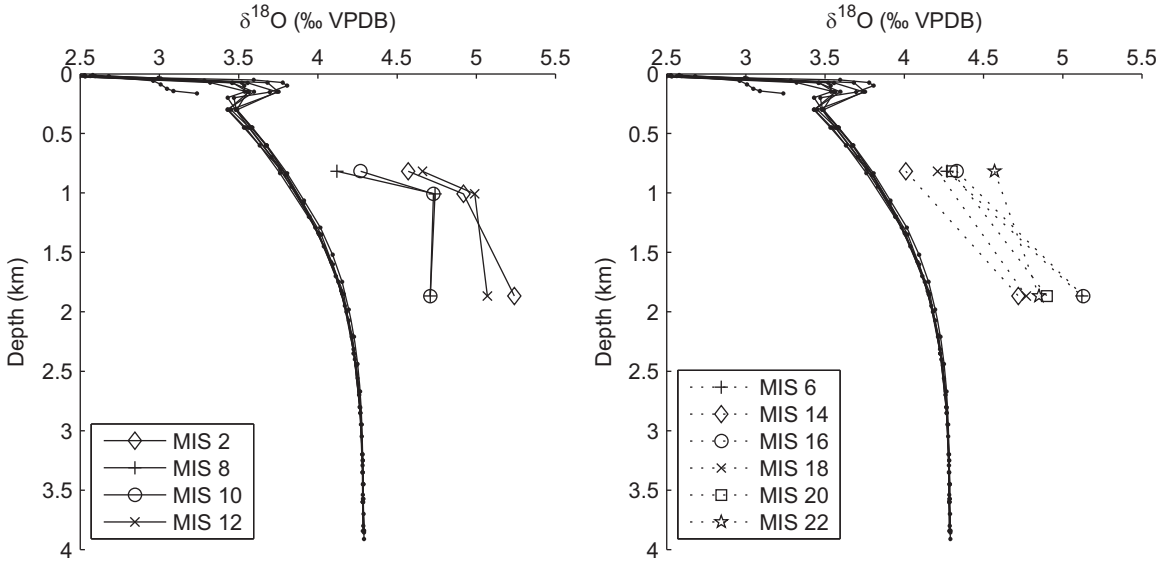

Fig. 7. Bering Sea $\delta^{18}O_c$ (Fig. 2) adjusted by +1.1‰ for the whole-ocean change since the LGM (Labeyrie et al., 2002) compared to maximum glacial $\delta^{18}O$ (Table 4). (Left) Glacial profiles from U1342 (819 m), U1345 (1008 m) and U1339 (1868 m). (Right) Glacial profiles from U1342 and U1339.

the slightly warmer and fresher water observed in the Bering Sea, compared to the open North Pacific (Roden, 1995). The relatively high $\delta^{18}O_C$ and high $\delta^{13}C_{DIC}$ values above 1000 m in the Okhotsk Sea shows the extent of the well-ventilated, chlorofluorocarbon-enriched, cold, nutrient-depleted brine (Wong et al., 1998). Deeper than around 1000 m, the Okhotsk Sea profiles are similar to the Emperor and Bering profiles.

The coretop *Uvigerina* $\delta^{18}O$ (Fig. 8a) is generally consistent with equilibrium offset corrected *Cibicidoides* (+0.5‰; Fontanier et al., 2006) at depths where there are data from both species. Coretop Emperor and Okhotsk $\delta^{18}O$ and Bering $\delta^{18}O$ >2 km are also broadly consistent with $\delta^{18}O_c$ in shape of the profile, where there is little vertical structure (Fig. 9a) and the values are slightly higher (0.1–0.2‰) than $\delta^{18}O_C$ (Fig. 9a). For Bering $\delta^{18}O$ <2 km, there is a larger offset of ~0.6‰ of the coretop data to more positive values from $\delta^{18}O_C$ (Figs. 8a and 9a).

The coretop $\delta^{13}C$ (Fig. 8b) is more variable than the $\delta^{18}O$ (compare standard deviations of offsets in Fig. 9a and b). The offset-corrected (+0.9‰; Mix et al., 1995) coretop *Uvigerina* $\delta^{13}C$ is consistent with *Cibicidoides*. The Emperor and Ohkotsk profiles as well as the Bering profile > 2 km are consistent with $\delta^{13}C_{DIC}$, where average offsets from $\delta^{13}C_{DIC}$ overlap with zero (Fig. 9b), and where the Bering $\delta^{13}C$ values are systematically more negative than the Emperor $\delta^{13}C$, similar to the modern $\delta^{13}C_{DIC}$ (Fig. 8b). Above 2 km, however, Bering $\delta^{13}C$ is offset to more positive values than $\delta^{13}C_{DIC}$ by ~0.4‰.

One possible contribution to the positive anomalies in both $\delta^{18}O$ and $\delta^{13}C$ at 500–2000 m water depth in the Bering Sea is the carbonate ion effect (Spero et al., 1997). The oxygen minimum zone is more intense in the Bering Sea, and is associated with a higher concentration of respired nutrients and carbon dioxide than in the Okhotsk Sea at these depths (Talley, 2007). This results in a lower carbonate ion concentration, and an expected increase in both $\delta^{18}O$ and $\delta^{13}C$ of equilibrium calcite, which is consistent with our observations. Though the carbonate ion effect is not known for the Bering and Okhotsk OMZs during the LGM, the sense of the bias would be the same for the $\delta^{18}O$ and $\delta^{13}C$, either both positive or both negative.

3.6. The LGM depth profiles

All of the LGM $\delta^{18}O$ profiles are offset to more positive values than the modern profile corrected for the whole-ocean change (+1.1‰; Labeyrie et al., 2002) (Figs. 8c and 9c). Keigwin (1998) observed that the Okhotsk $\delta^{18}O$ in both *Uvigerina* and *Cibicidoides* decreases by 0.5–0.6‰ from 2000 to 1000 m water depth, a steeper gradient than the modern $\delta^{18}O_C$. This can be seen in the larger average offset of $\delta^{18}O$ from $\delta^{18}O_C$ for Okhotsk than Emperor and the decreasing [$\delta^{18}O$–$\delta^{18}O_C$] with decreasing $\delta^{18}O_C$ (Fig. 9c). In the Bering Sea, the water column is not as well sampled as in the Okhotsk and Emperor study areas, but it appears that the shape of the profile was also different than the modern. The $\delta^{18}O$ is relatively uniform from 3200 m water depth to ~1500–2000 m water depth, and decreases ~0.5‰ by 700 m water depth.

The LGM Bering $\delta^{13}C$ profile is relatively uniform from 700 to 3200 m water depth, in contrast to the modern profile, which gradually decreases by 0.5‰ from 4000 to 500 m. This is also in contrast to the Okhotsk profile, where both *Uvigerina* and *Cibicidoides* decrease by 0.5‰ from 2000 to 1000 m water depth. The Emperor $\delta^{13}C$ is very similar to the modern $\delta^{13}C_{DIC}$ corrected for the whole-ocean change (–0.32‰; Duplessey et al., 1988).

4. Discussion

4.1. The Holocene-LGM profiles

Keigwin (1998) interpreted the relatively high LGM Emperor $\delta^{18}O$ of *Cibicidoides* as indicating a colder and saltier deep water than today. This is consistent with estimates of the θ and S based on porewater profiles of chlorinity and $\delta^{18}O_W$ that show that density differences in the LGM ocean were dominated by salinity, and that the deep ocean was near its freezing point (Adkins et al., 2002). The $\delta^{18}O$ in the deep LGM Bering Sea is similar but slightly higher than Emperor values and uniform, showing that this cold and salty deep water may also have filled the deep Bering Sea. This deep water appeared poorly ventilated, based on benthic-planktonic radiocarbon age differences from the eastern equatorial Pacific (Shackleton et al., 1988) and Gulf of Alaska (Galbraith et al., 2007; Davies-Walczak et al., 2014).

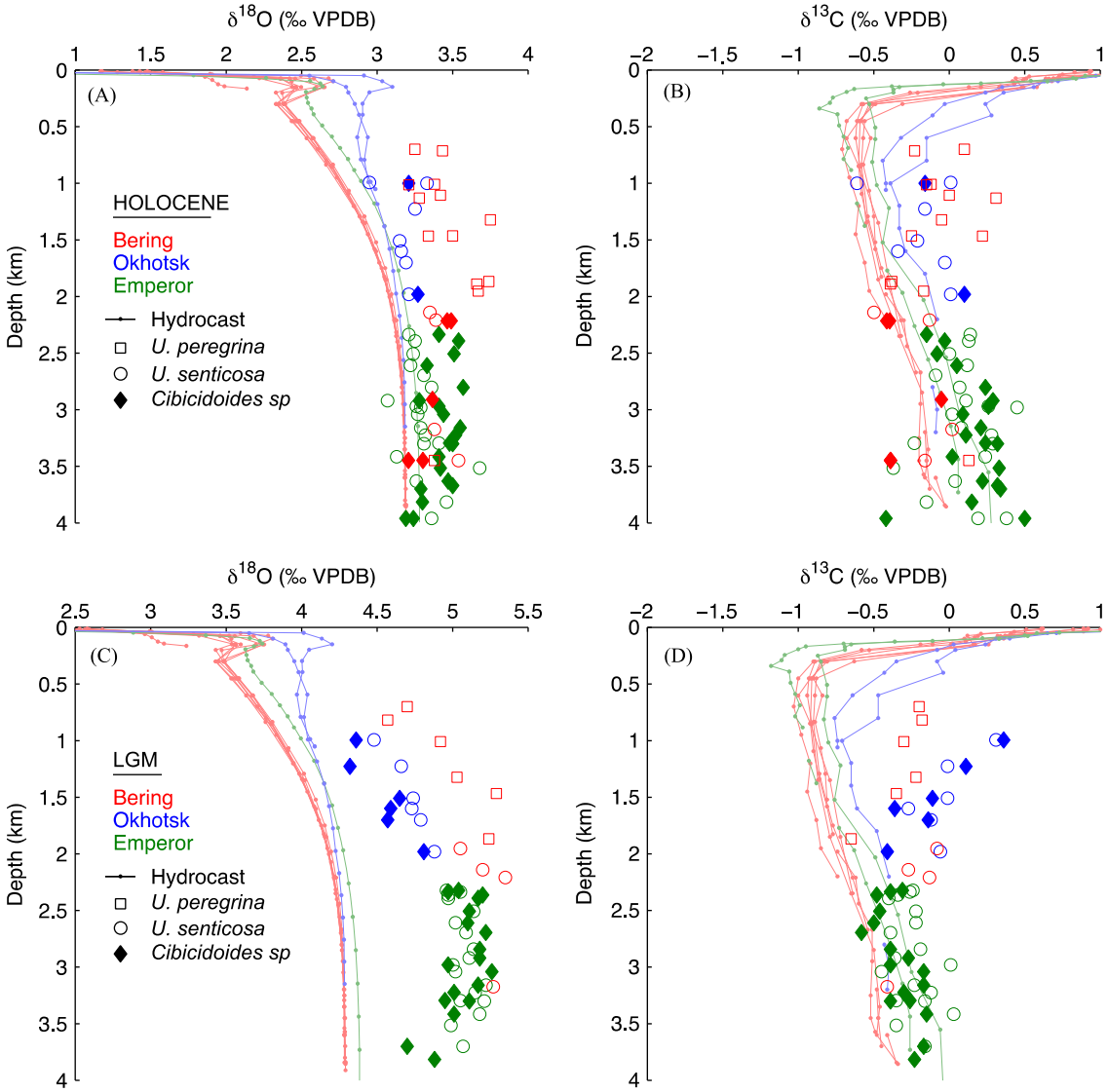

Fig. 8. Holocene and LGM profiles from the Bering Sea (Table 3), Okhotsk Sea and Emperor Seamounts (Keigwin, 1998). The *Cibicioides* have been corrected by +0.5‰ in for offset of $\delta^{18}O$ from equilibrium (Fontanier et al., 2006). The *U. senticosa* have been corrected for $\delta^{13}C$ offset from *U. peregrina* (Table 1 and Fig. 5). We correct the *Uvigerina* $\delta^{13}C$ data by +0.9‰ (Mix, 1995). (a) The equilibrium calcite $\delta^{18}O$ ($\delta^{18}O_c$ corrected to VPDB) from Fig. 2e plotted with Holocene benthic foraminiferal $\delta^{18}O$. (b) The $\delta^{13}C_{DIC}$ from hydrocasts (Fig. 1) plotted with Holocene benthic foraminiferal $\delta^{13}C$. (c) The $\delta^{18}O_c$ adjusted by +1.1‰ for the whole-ocean change since the LGM (Labeyrie et al., 2002), plotted with the benthic foraminiferal maximum $\delta^{18}O$ from the LGM. (d) The $\delta^{13}C_{DIC}$ adjusted by −0.32‰ for the whole ocean change since the LGM (Duplessey et al., 1988), plotted LGM benthic foraminiferal $\delta^{13}C$.

The LGM divide between the poorly-ventilated deep water below and the well-ventilated intermediate water above is at ~2000 m in the Okhotsk Sea, similar to $\delta^{13}C$ profiles from sites further south at the Japan Margin (Matsumoto et al., 2002), Ontong Java Plateau (Herguera et al., 1992), and Gulf of California (Keigwin, 2002). If we take the Bering stable isotope data from <2000 m at face value, the $\delta^{18}O$ is ~0.3‰ higher and the *Uvigerina* $\delta^{13}C$ is up to ~0.5‰ lower than in the Okhotsk above the divide. Even though the potential bias in these OMZ-depth data due to the carbonate ion effect is unknown, since the Bering–Okhotsk isotopic difference has a different sign for $\delta^{18}O$ as $\delta^{13}C$, it is clear that the water masses <2000 m had distinct compositions in the two basins.

4.2. The LGM in the subarctic Pacific

Though we don't fully understand the difference between the Holocene Bering foraminiferal stable isotopes and hydrography, or whether this difference varied through time, it is instructive to examine possible implications of the LGM profiles.

If we consider the scenario where intermediate water was produced only in the Okhotsk Sea then flowed into the Bering Sea, then it would require that Okhotsk water $\delta^{18}O$ be modified in transit through mixing with cooler and/or saltier water, since the Bering $\delta^{18}O$ <2 km is 0.3‰ more positive than the Okhotsk. This could happen if the newly ventilated Okhotsk water entrained some of the deep, high-$\delta^{18}O$ water mass as it passed through the straits in the Kuril and Aleutian Islands, where WOCE transects show intense tidal mixing (Freeland et al., 1998; Roden, 1995), and transport of water properties in mesoscale eddies (Maslowski et al., 2008). We can predict this modification would result in the low-$\delta^{18}O$ water in the Bering Sea to have $\delta^{13}C$ intermediate in value between the Okhotsk and Emperor values. The Bering $\delta^{13}C$ does not appear to show this enrichment in $\delta^{13}C$ (Figs. 8d and 9), but rather, maintains low values similar to that of the glacial deep water. This water mass mixing argument would hold even if the Bering stable isotope data <2 km

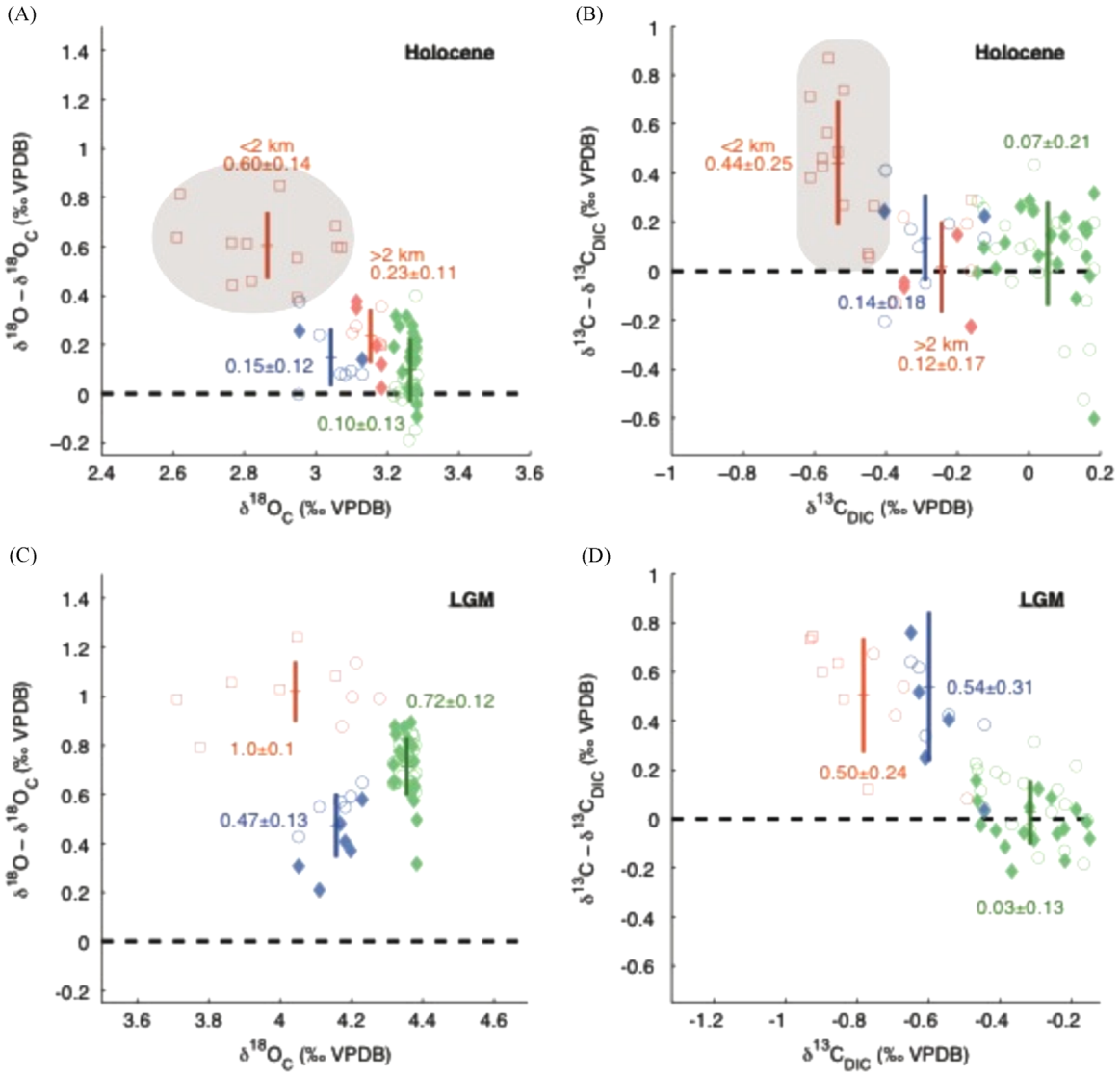

Fig. 9. Benthic foraminiferal stable isotope offsets from the hydrographic reference curves. Each symbol shows the difference between a stable isotope measurement in Fig. 8 (including any associated species offset) and the mean value of the hydrocast reference curves for that water depth (for panels c and d, including the adjustment for the whole-ocean change since the LGM). The colors and symbols are the same as in Fig. 8, and the four panels here correspond to the four panels in Fig. 8. The thick lines and annotations show the mean and standard deviation of values from each study area. In panels a and b, the mean and standard deviation of Bering Sea data <2 km water depth (enclosed by gray shading) are calculated separately from the data >2 km water depth. (For interpretation of the references to color in this figure legend, the reader is referred to the web version of this article.)

Table 2
Age model for U1339 and U1345, based on wiggle-matching the benthic $\delta^{18}O$ stratigraphy to the Lisiecki and Raymo (2005) stack.

	Stack		U1345		U1339	
	End (ka)	Start (ka)	Top (mbsf)	Bottom (mbsf)	Top (mbsf)	Bottom (mbsf)
MIS 1	0	14	-0.5 ± 1	6.0 ± 0.5	-0.5 ± 1	3.5 ± 0.5
MIS 5	71	130	23.6 ± 1	35.2 ± 1.5	20.5 ± 1	34.6 ± 1
MIS 7	191	243	47.8 ± 1	68.7 ± 1	54.2 ± 1	70.5 ± 1.5
MIS 9	300	337	87.0 ± 2	98.6 ± 3	83.2 ± 2	91.8 ± 1
MIS 11	374	424	115.3 ± 2	130.6 ± 2	98.5 ± 1	112.0 ± 1.5
MIS 13	478	533	148.7 ± 2		123.7 ± 2	135.9 ± 1.5
MIS 15	565	621			141.5 ± 1.5	154.7 ± 1
MIS 17	676	712			164.5 ± 1.5	171.2 ± 1
MIS 19	761	790			176.8 ± 2	185.0 ± 1
MIS 21	814	866			194.0 ± 2	205.2 ± 2

water depth were translated to more positive or more negative values due to the carbonate ion effect.

Alternatively, if we consider the scenario where the Okhotsk did not produce intermediate water, but was downstream of a Bering Sea source, then it would require that the low-$\delta^{18}O$ water be modified by -0.3‰ by mixing with warmer and/or fresher water by the time it reaches the Okhotsk Sea. This modification would also need to be accompanied by an increase in $\delta^{13}C$ of up to

Table 3
Uvigerina Holocene and LGM time slice data from this study, 17JPC (Brunelle et al., 2007), 51JPC and 57JPC (Cook et al., 2011), U1340 (Schlung et al., 2013), U1341 (Sakamoto, personal communication), U1342 (Knudson and Ravelo, 2015), U1343 (Asahi, personal communication), and U1344 (Okazaki, personal communication), HLY02-02 multicore data are of Rose-Bengal stained foraminifera. These are the original data, without species–species offset corrections.

Core name	Water depth (m)	Species	Holocene			LGM		
			Core Depth (m)	$\delta^{13}C$ (‰ VPDB)	$\delta^{18}O$ (‰ VPDB)	Core Depth (m)	$\delta^{13}C$ (‰ VPDB)	$\delta^{18}O$ (‰ VPDB)
HLY02-02-57JPC	700	*U. peregrina*	0.05	−0.80	3.25	0.88	−1.10	4.70
HLY02-02-24MC	714	*U. peregrina*	0.01	−1.13	3.43	—	—	—
U1342	819	*U. peregrina*	—	—	—	0.55	−1.08	4.57
U1345	1008	*U. peregrina*	0.01	−1.02	3.38	7.36	−1.20	4.92
HLY02-02-56MC	1015	*U. peregrina*	0.01	−1.05	3.21	—	—	—
HLY02-02-2MC	1105	*U. peregrina*	0.01	−0.90	3.42	—	—	—
HLY02-02-3JPC	1132	*U. peregrina*	0.08	−0.59	3.28	—	—	—
HLY02-02-50MC	1456	*U. peregrina*	0.01	−1.15	3.50	—	—	—
U1340	1295	*U. peregrina*	−0.04	−0.95	3.75	2.10	−1.12	5.03
HLY02-02-51JPC	1467	*U. peregrina*	0.12	−0.68	3.34	3.76	−1.25	5.29
U1339	1868	*U. peregrina*	0.01	−1.28	3.74	5.34	−1.55	5.24
HLY02-02-43MC	1889	*U. peregrina*	0.01	−1.29	3.66	—	—	—
U1343	1953	*U. peregrina*	0.01	−1.07	3.67	4.23	−0.68	5.05
		U. senticosa						
U1341	2140	*U. senticosa*	0.65	−1.10	3.35	2.15	−0.87	5.20
HLY02-02-17JPC	2209	*U. senticosa*	0.20	−0.73	3.39	2.82	−0.73	5.35
HLY02-02-16MC	2216	*C. mundulus*	0.01	−0.39	2.99	—	—	—
		C. mundulus		−0.41	2.96			
HLY02-02-31MC	2910	*C. kullenbergi*	0.01	−0.05	−2.87	—	—	—
U1344	3173	*U. senticosa*	0.01	−0.58	3.38	8.71	−1.01	5.27
HLY02-02-5MC	3449	*U. peregrina*	0.01	−0.77	3.38	—	—	—
		U. senticosa		−0.76	3.54			
		Cibicidoides sp.		−0.39	2.80			
		Cibicidoides sp.		−0.39	2.71			

Table 4
Uvigerina time slice data.

	U1342 (819 m)		U1345 (1008 m)		U1339 (1868 m)	
	Core depth (m)	$\delta^{18}O$ (‰ VPDB)	Core depth (m)	$\delta^{18}O$ (‰ VPDB)	Core depth (m)	$\delta^{18}O$ (‰ VPDB)
MIS 2	0.55	4.57	7.36	4.92	5.34	5.24
MIS 6	139.92	4.27			35.85	5.12
MIS 8	247.03	4.12	71.24	4.74	71.39	4.71
MIS 10	339.56	4.27	101.66	4.73	93.25	4.71
MIS 12	432.20	4.66	134.23	4.99	112.53	5.07
MIS 14	532.09	4.01			137.83	4.72
MIS 16	629.86	4.33			156.71	5.13
MIS 18	715.44	4.21			172.30	4.77
MIS 20	798.25	4.30			187.97	4.90
MIS 22	877.46	4.57			207.18	4.85

0.5‰. This $\delta^{13}C$ increase is in the opposite direction than would be expected from water mass aging and input of low-$\delta^{13}C$ respired organic matter, and seems unlikely, even if the Bering stable isotope data were translated to more positive or more negative values due to the carbonate ion effect.

A third alternative is that the Bering Sea and Okhotsk Sea both produced relatively well-ventilated intermediate water during the LGM. There is evidence of expanded LGM sea ice compared to today in both the Bering (Sancetta and Robinson, 1983; Katsuki and Takahashi, 2005) and Okhotsk (Okazaki et al., 2005) Seas. The surface waters in the two basins may have different isotopic composition because of differences in the hydrological cycle, local productivity and air–sea gas exchange resulting in distinct preformed $\delta^{18}O$ and $\delta^{13}C$.

Based on the distribution of *C. davisiana*, Tanaka and Takahashi (2005) argued that solely the Bering Sea was a source of intermediate water during MIS2. However, if dense water formed in both marginal seas, one possibility is that the Bering Sea source water was formed during sea ice formation, and was therefore associated with the hydrography favorable for high abundance of *C. davisiana*, while Okhotsk source water was associated with a different process. It is also possible that the distinct water mass in the Okhotsk originated elsewhere.

The $\delta^{13}C_{DIC}$ of surface ocean water varies spatially, depending on biological uptake and air–sea carbon dioxide exchange (Lynch-Stieglitz et al., 1995), where $\delta^{13}C_{DIC}$ is enriched with biological productivity, but also enriched with lower sea surface temperatures and depleted with carbon dioxide invasion into the surface ocean. During the LGM, productivity was low in both the Okhotsk and Bering Seas (Kohfeld and Chase, 2011), possibly due to expanded sea ice, which also would limit air–sea gas exchange, though in the Bering Sea, seasonal ice did not appear to reach as far into the center of the basin as the Bowers Ridge (Katsuki and Takahashi, 2005). Differences in LGM ice extent, productivity and air–sea exchange between the Okhotsk and Bering Seas could result in different surface water $\delta^{13}C$, and therefore different preformed $\delta^{13}C_{DIC}$ of newly-ventilated intermediate water.

The $\delta^{18}O_W$ of modern precipitation in the Okhotsk Sea is a few permil lower than in the Bering Sea, because of the slightly cooler temperatures in the Okhotsk, and the influence of the land masses that surround this marginal sea on three sides (Bowen and Revenaugh, 2003). The modern $\delta^{18}O_W$ of surface water is slightly lower in the Okhotsk Sea, but similar in the two basins, both showing the strong influence of seasonal sea ice, and a shallow slope to the $\delta^{18}O_W$-salinity relationship (LeGrande and Schmidt, 2006). This difference between the precipitation and surface water $\delta^{18}O_W$ of these two basins is the same sense as the difference between the $\delta^{18}O_W$ profiles above 2000 m water depth, where the Bering is higher than the Okhotsk.

4.3. Glacial–interglacial patterns

The benthic $\delta^{18}O$ data show that the structure of the water column differs between glacials and today (Fig. 7). The glacial–interglacial amplitude of the U1339 record (1870 m) is similar to the global benthic stack, while the amplitude of U1342 (819 m) is smaller, resulting in more negative glacial maxima in $\delta^{18}O$ (Figs. 6 and 7). Knudson and Ravelo (2015) interpret this lower glacial $\delta^{18}O$ as a well-ventilated glacial intermediate water mass that formed locally during brine rejection. They argue that the $\delta^{18}O_W$ at this site was higher during interglacials when, like today, the water at this site was strongly influenced by high-$\delta^{18}O$ deep water that originated in the Southern Hemisphere. During glacials, enhanced sea-ice formation would have produced dense water with little oxygen isotope fractionation (Tan and Strain, 1996). The newly-produced water would therefore carry the relatively low $\delta^{18}O$ signature of high-latitude surface water.

The benthic $\delta^{18}O$ gradient between U1342 and U1339 ranges from 0.4‰ to 0.8‰ (Fig. 7, Table 4), larger than the difference in calculated equilibrium calcite of 0.3‰ between 820 and 1870 m in the modern Bering Sea (Fig. 7). Today water at 1870 m, the depth of U1339, is in the core of PDW, and water at 820 m, the depth of U1342, is a mixture of PDW and NPIW. The 26.8 σ_θ isopycnal at the core of NPIW in the Bering Sea is quite shallow, at 250–300 m (MacDonald et al., 2001). The larger gradient between these two coring depths during glaciations is consistent with an expanded, well-ventilated intermediate water mass that reached the U1342 coring site.

Site U1345 (1008 m) can constrain the depth of the hydrographic boundary between the apparently well-ventilated water above recorded by U1342 and the more poorly-ventilated water below recorded by U1339. During glacials MIS 8, 10 and 12 the $\delta^{18}O$ in U1345 is similar to U1339 (Fig. 6), suggesting that the hydrographic boundary was above 1008 m, and the water column from 1008 to 1870 m was homogeneous. During MIS 2, the $\delta^{18}O$ in U1345 was ~0.2‰ lower than at U1339, suggesting that the well-ventilated water penetrated more deeply during this glaciation.

5. Conclusions

We use multi-species benthic stable isotope measurements in two sites from the IODP Expedition to the Bering Sea to assess the structure of the water column during the late Pleistocene. There is a hydrographic divide between relatively high $\delta^{18}O$ water below and low $\delta^{18}O$ water above during glaciations, which was near or above ~1000 m water depth. The upper water mass may be relatively well-ventilated, with a low $\delta^{18}O$ signature that could be the result of formation through brine rejection. In a closer look at the LGM, we find that the upper Bering Sea water column is relatively enriched in ^{18}O and depleted in ^{13}C compared to the Okhotsk Sea. The distinct isotopic signatures in the two marginal seas may indicate that well-ventilated water formed in both basins. These observations suggest that in the late Pleistocene, the glacial circulation of the subarctic Pacific was systematically different than today, with implications for the global heat budget.

Acknowledgments

We are grateful to Meredith Annex, Claire Baecher, Miranda Bona, Kalila Booker-Cassano, Galen Corey, Zara Currimjee, Paul Deaderick, Thomas Gaidus, Kathryn Kumamoto, Julia Matejcek, Molly McEntee, Harper Robertson and Susan Trimarchi at Williams College for their help in sample preparation, and Andy Ross, June Padman and Nancy Kyle at OSU, and Dyke Andreassen and Ting Hsieh at UCSC for assistance in sample analysis. Dan McCorkle generously provided the HLY02-02 multicore and hydrocast data and valuable discussions. We thank Hirofumi Asahi, Yusuke Okazaki and Tatsuhiko Sakamoto for providing unpublished data for the LGM time slice. We also thank two anonymous reviewers whose comments helped to improve this manuscript. Support for this project was from the Consortium for Ocean Leadership, the National Science Foundation Grant #0963114 and the Williams College Divisional Research Funding committee.

References

Adkins, J.F., McIntyre, K., Schrag, D.P., 2002. The salinity, temperature, and $\delta^{18}O$ of the glacial deep ocean. Science 298, 1769–1773.

Asahi, H.S., Kende, S., Ikehara, M., Sakamoto, T., Takahashi, K., Ravel, A.C., Alvarez-Zarikian, C.A., Khim, B.K., Leng, M.J., 2016. Orbital-scale benthic foraminiferal oxygen isotope stratigraphy at the northern Bering Sea slope site U1343 (IODP Expedition 323) and its Paleistocene paleoceanographic significance. Deep-Sea Res. Part II, 125-126, 66–83. http://dx.doi.org/10.1016/j.dsr2.2014.01.004.

Bowen, Gabriel, J., Revenaugh, J., 2003. Interpolating the isotopic composition of modern meteoric precipitation. Water Resour. Res. 39, 1299.

Brunelle, B.G., Sigman, D.M., Cook, M.S., Keigwin, L.D., Haug, G.H., Plessen, B., Schettler, G., Jaccard, S.L., 2007. Evidence from diatom-bound nitrogen isotopes for subarctic Pacific stratification during the last ice age and a link to North Pacific denitrification changes. Paleoceanography 22, PA1215.

Cook, M.S., Keigwin, L.D., Birgel, D., Hinrichs, K.-U., 2011. Repeated pulses of vertical methane flux recorded in glacial sediments from the southeast Bering Sea. Paleoceanography 26, PA2210.

Coplen, T.B., 1988. Normalization of oxygen and hydrogen isotope data. Chem. Geol. Isotope Geoscience section 72 (4), 293–297.

Corliss, B.H., Emerson, S.R., 1990. Distribution of Rose Bengal stained deep-sea benthic foraminifera from the Nova Scotian continental margin and Gulf of Maine. Deep Sea Res. 37, 381–400.

Davies-Walczak, M., Mix, A.C., Stoner, J.S., Southon, J.R., Cheseby, M., Xuan, C., 2014. Late Glacial to Holocene radiocarbon constraints on North Pacific Intermediate Water ventilation and deglacial atmospheric CO_2 sources. Earth Planet. Sci. Lett. 397, 57–66.

Duplessy, J.-C., Shackleton, N.J., Fairbanks, R.G., Labeyrie, L., Oppo, D., Kallel, N., 1988. Deepwater source variations during the last climatic cycle and their impact on the global deepwater circulation. Paleoceanography 3, 343–360.

Eakins, B.W., Sharman, G.F., 2010. Volumes of the World's Oceans from ETOPO1. NOAA National Geophysical Data Center, Boulder, CO.

Emile-Geay, J., Cane, M.A., Naik, N., Seager, R., Clement, A.C., van Geen, A., 2003. Warren revisited: atmospheric freshwater fluxes and "Why is no deep water formed in the North Pacific". J. Geophys. Res. 108, 3178.

Fontanier, C., Mackensen, A., Jorissen, F.J., Anschutz, P., Licari, L., Griveaud, C., 2006. Stable oxygen and carbon isotopes of live benthic foraminifera from the Bay of Biscay: microhabitat impact and seasonal variability. Mar. Micropaleontol. 58 (3), 159–183.

Freeland, H.J., Bychkov, A.S., Whitney, F., Taylor, C., Wong, C.S., Yurasov, G.I., 1998. WOCE section P1W in the Sea of Okhotsk 1. Oceanographic data description. J. Geophys. Res. 103, 15613–15623.

Galbraith, E.D., Jaccard, S.L., Pedersen, T.F., Sigman, D.M., Haug, G.H., Cook, M., Southon, J.R., Francois, R., 2007. Carbon dioxide release from the North Pacific abyss during the last deglaciation. Nature 449, 890–893.

Herguera, J.C., Berger, W.H., Jansen, E., 1992. Evidence for a bathyal front at 2000 m depth in the glacial Pacific, based on a depth transect on Ontong Java Plateau. Paleoceanography 7, 273–288.

Herguera, J.C., Paull, C.K., Perez, E., Ussler, W., Peltzer, E., 2014. Limits to the sensitivity of living benthic foraminifera to pore water carbon isotope anomalies in methane vent environments. Paleoceanography 29 (3), 273–289.

Horikawa, K., Asahara, Y., Yamamoto, K., Okazaki, Y., 2010. Intermediate water formation in the Bering Sea during glacial periods: evidence from neodymium isotope ratios. Geology 38, 435–438.
Katsuki, K., Takahashi, K., 2005. Diatoms as paleoenvironmental proxies for seasonal productivity, sea-ice and surface circulation in the Bering Sea during the late Quaternary. Deep Sea Res. Part II 52, 2110–2130.
Keigwin, L.D., 1998. Glacial-age hydrography of the far Northwest Pacific Ocean. Paleoceanography 13, 323–339.
Keigwin, L.D., 2002. Late Pleistocene–Holocene paleoceangraphy and ventilation of the Gulf of California. J. Oceanogr. 58, 421–432.
Key, R.M., Quay, P.D., Schlosser, P., McNichol, A.P., von Reden, K.F., Schneider, R.J., Elder, K.L., Stuiver, M., Östlund, H.G., 2002. WOCE radiocarbon IV: Pacific Ocean results; P10, P13N, P14C, P18, P19, S4P. Radiocarbon 44, 239–392.
Knudson, K., Ravelo, A.C., 2015. North Pacific Intermediate Water circulation enhanced by the closure of the Bering Strait. Paleoceanography 30 (10), 1287–1304.
Kohfeld, K.E., Chase, Z., 2011. Controls on deglacial changes in biogenic fluxes in the North Pacific Ocean. Quat. Sci. Rev. 30, 3350–3363.
Labeyrie, L., Waelbroeck, C., Duplessy, J.-C., 2002. Constraints on the ocean oxygen isotopic enrichment between the Last Glacial Maximum and the Holocene: Paleoceanographic implications. Quat. Sci. Rev. 21, 315–330.
Leduc, G., Vidal, L., Tachikawa, K., Rostek, F., Sonzogni, C., Beaufort, L., Bard, E., 2007. Moisture transport across Central America as a positive feedback on abrupt climatic changes. Nature 445, 908–911.
LeGrande, A.N., Schmidt, G.A., 2006. Global gridded data set of the oxygen isotopic composition in seawater. Geophys. Res. Lett. 33, L12604.
Lehmann, M.F., Sigman, D.M., McCorkle, D.C., Brunelle, B.G., Hoffmann, S., Kienast, M., Cane, G., Clement, J., 2005. Origin of the deep Bering Sea nitrate deficit: constraints from the nitrogen and oxygen isotopic composition of water column nitrate and benthic nitrate fluxes 19. GB4, 005.
Lisiecki, L.E., Raymo, M.E., 2005. A Pliocene–Pleistocene stack of 57 globally distributed benthic $\delta^{18}O$ records. Paleoceanography 20, PA1003.
Lynch-Stieglitz, J., Stocker, T.F., Broecker, W.S., Fairbanks, R.G., 1995. The influence of air-sea exchange on the isotopic composition of oceanic carbon: observations and modeling. Glob. Biogeochem. Cycles 9, 653–665.
MacDonald, A.M., Suga, T., Curry, R.G., 2001. An isopycnally averaged North Pacific climatology. J. Atmos. Ocean. Technol. 18, 394–420.
Maslowski, W., Roman, R., Kinney, J.C., 2008. Effects of mesoscale eddies on the flow of the Alaskan Stream. J. Geophys. Res.: Ocean. 113 (C7).
Matsumoto, K., Oba, T., Lynch-Stieglitz, J., Yamamoto, H., 2002. Interior hydrography and circulation of the glacial Pacific Ocean. Quat. Sci. Rev. 21, 1693–1704.
McCorkle, D.C., Corliss, B.H., Farnham, C.A., 1997. Vertical distributions and stable isotopic compositions of live (stained) benthic foraminifera from the North Carolina and California continental margins. Deep Sea Res. 44, 983–1024.
McCorkle, D.C., Keigwin, L.D., Corliss, B.H., Emerson, S.R., 1990. The influence of microhabitats on the carbon isotopic composition of deep-sea benthic foraminifera. Paleoceanography 5, 161–185.
McNichol, A.P., Jones, G.A., Hutton, D.L., Gagnon, A.R., 1994. The rapid preparation of seawater TCO_2 for radiocarbon analysis at the National Oceanic and Atmospheric Sciences AMS Facility. Radiocarbon 36, 237–246.
Mix, A.C., Pisias, N.G., Rugh, W., Wilson, J., Morey, A., Hagelberg, T.K., 1995. Benthic foraminifer stable isotope record from Site 849 (0–5 Ma): local and global climate changes. Proc. Ocean. Drill. Program, Sci. Results 138, 371–412.
Ohkushi, K., Itaki, T., Nemoto, N., 2003. Last glacial-Holocene change in intermediate-water ventilation in the Northwestern Pacific. Quat. Sci. Rev. 22, 1477–1484.
Okazaki, Y., Takahashi, K., Katsuki, K., Ono, A., Hori, J., Sakamoto, T., Uchida, M., Shibata, Y., Ikehara, M., Aoki, K., 2005. Late Quaternary paleoceanographic changes in the southwestern Okhotsk Sea: evidence from geochemical, radiolarian, and diatom records. Deep. Sea Res. Part II 52, 2332–2350.
Ostermann, D.R., Curry, W.B., 2000. Calibration of stable isotopic data: an enriched $\delta^{18}O$ standard used for source gas mixing detection and correction. Paleoceanography 15 (3), 353–360.
Pierre, C., Blanc-Valleron, M.M., Caquineau, S., März, C., Ravelo, A.C., Takahashi, K., Zarikian, C.A., 2016. Mineralogical, geochemical and isotopic characterization of authigenic carbonates from the methane-bearing sediments of the Bering Sea continental margin (IODP Expedition 323, Sites U1343–U1345). Deep Sea Res. Part II: Topical Studies in Oceanography 125-126, 133–144. http://dx.doi.org/10.1016/j.dsr2.2014.03.011.
Rella, S.F., Tada, R., Nagashima, K., Ikehara, M., Itaki, T., Ohkushi, K.I., Sakamoto, T., Harada, N., Uchida, M., 2012. Abrupt changes of intermediate water properties on the northeastern slope of the Bering Sea during the last glacial and deglacial period. Paleoceanography 27, 3.
Roden, G.I., 1995. Aleutian Basin of the Bering Sea: thermohaline, oxygen, nutrient, and current structure in July 1993. J. Geophys. Res. 100, 13,539–13,554.
Sancetta, C., Robinson, S.W., 1983. Diatom evidence on Wisconsin and Holocene events in the Bering Sea. Quat. Res. 20, 232–245.
Schlung, S.A., Ravelo, A.C., Aiello, I.W., Andreasen, D.H., Cook, M.S., Drake, M., Dyez, K.A., Guilderson, T.P., LaRiviere, J.P., Stroynowski, Z., Takahashi, K., 2013. Millennial-scale climate change and intermediate water circulation in the Bering Sea from 90 ka: a high-resolution record from IODP Site U1340. Paleoceanography 28, 54–67.
Schrag, D.P., Adkins, J.F., McIntyre, K., Alexander, J., Hodell, D.A., Charles, C.D., McManus, J.F., 2002. The oxygen isotopic composition of seawater during the Last Glacial Maximum. Quat. Sci. Rev. 21, 331–342.
Shackleton, N.J., 1974. Attainment of isotopic equilibrium between ocean water and the benthonic foraminifera genus Uvigerina: isotopic changes in the ocean during the last glacial. In: Les méthodes quantitatives d'étude des variations du climat au cors du Pléistocène. Colloques Internationaux du C. N. R. S., #219.
Shackleton, N.J., Duplessy, J.-C., Arnold, M., Maurice, P., Hall, M.A., Cartlidge, J., 1988. Radiocarbon age of last glacial Pacific deep water. Nature 335, 708–711.
Shcherbina, A.Y., Talley, L.D., Rudnick, D.L., 2003. Direct observations of North Pacific ventilation: brine rejection in the Okhotsk Sea. Science 302, 1952–1955.
Smith, W.H., Sandwell, D.T., 1997. Global sea floor topography from satellite altimetry and ship depth soundings. Science 277 (5334), 1956–1962.
Spero, H.J., Bijma, J., Lea, D.W., Bemis, B.E., 1997. Effect of seawater carbonate concentration on foraminiferal carbon and oxygen isotopes. Nature 390 (6659), 497–500.
Takahashi, K., Ravelo, A.C., Alvarez Zarikian, C., Scientists, E., 2011. In: Proceedings of the Integrated Ocean Drilling Program, Expedition 323. Tokyo.
Tanaka, S., Takahashi, K., 2005. Late Quaternary paleoceanographic changes in the Bering Sea and the western subarctic Pacific based on radiolarian assemblages. Deep. Sea Res. Part II: Top. Stud. Oceangr. 52 (16), 2131–2149.
Talley, L.D., 2003. Shallow, intermediate, and deep overturning components of the global heat budget. J. Phys. Oceanogr. 33, 530–560.
Talley, L.D., 2007. Hydrographic atlas of the World Ocean Circulation Experiment (WOCE): Volume 2: Pacific Ocean. In: Sparrow, M.D., Chapman, P., Gould, J. (Eds.), WOCE International Project Office.
Tan, F.C., Strain, P.M., 1996. Sea ice and oxygen isotopes in Foxe Basin, Hudson Bay, and Hudson Strait, Canada. J. Geophys. Res. 101, 20,869–20,876.
Van Scoy, K.A., Olson, D.B., Fine, R.A., 1991. Ventilation of North Pacific Intermediate Waters: the role of the Alaskan Gyre. J. Geophys. Res. 96, 16,801–816,810.
Warren, B.A., 1983. Why is no deep water formed in the North Pacific? J. Mar. Res. 41, 327–347.
Wehrmann, L.M., Risgaard-Petersen, N., Schrum, H.N., Walsh, E.A., Huh, Y., Ikehara, M., Pierre, C., D'Hondt, S., Ferdelman, T.G., Ravelo, A.C., Takahashi, K., Alvarez-Zarikian, C., 2011. The Integrated Ocean Drilling Program Expedition 323 Scientific Party, 2011. Coupled organic and inorganic carbon cycling in the deep subseafloor sediment of the northeastern Bering Sea Slope (IODP Exp. 323). Chem. Geol. 284 (3), 251–261.
Wessel, P., Smith, W.H.F., 1998. New, improved version of Generic Mapping Tools released. EOS Trans. Am. Geophys. Union 79, 579.
Wong, C.S., Matear, R.J., Freeland, H.J., Whitney, F.A., Bychkov, A.S., 1998. WOCE line P1W in the Sea of Okhotsk: 2. CFCs and the formation rate of intermediate water. J. Geophys. Res. 103, 15,625–15,642.